

## **Open thermodynamic systems: convection and similar processes modeling by the fluids bubble boiling method**

Anzor Gvelesiani

*Iv. Javakhishvili Tbilisi State University, M. Nodia Institute of Geophysics*  
1, Alexidze Str., 0171 Tbilisi, Georgia, e-mail:  
<anzor\_gvelesiani@yahoo.com>

### *Abstract*

*It is continued study of convective motions in different liquid geophysical environments by the novel solutions bubble-boiling modeling method, suggested in [1-3]. This method used with purpose of modeling of one- two- or three-dimensional convection in conditions of usual laboratory is appeared quite acceptable to consider: (a) the global planetary scale circulations; (b) surface mixed layer of oceans; (c) analogy between brittle failure and statistical physics, bubble nucleation leading to boiling; (d) peculiarities of thermal waters in northern glacial regions; (e) mantle convection in the Earth. The laboratory investigation of the subject, energetic analysis and details will be reported on other occasions.*

### **I. Introduction.**

The purpose of this article is to analyse well-known investigations of vertical, one-dimensional convective motions in nature and laboratory, on the base of our new experimental results [1-27]. Corresponding works will be considered in following order: global climate system – the Earth, the Sun, and space; atmosphere, ocean, thermal waters, volcanoes, geysers, jökulhlaup, Earth's mental plume, magnetosphere-ionosphere convection, laboratory experiments, examples of similar phenomena from adjacent science branches. These 1d-motions of the fluids, caused by heating below, according to well-known works have important role in convective motions of all extra-ordinal phenomena, and, naturally, in laboratory modeling experiments by means of solutions bubble boiling method [1-3], according to which consideration of only vertical motions is quite enough for description of the thermals behavior – the air-vapour bubbles in atmosphere, ocean, thermal waters, mantle-plumes, volcanoes, etc. – subject to action of weight and Archimedes forces [1].

In modeling laboratory experiments, it is obtained optimal relations between volume of investigated liquid and intensity of heat flux, identical length scales, and timescales of observations.

### **II. Soil-vegetation-atmosphere transfer schemes and hydrological models [5-10].**

**2.1.** Let's begin a consideration of the problem] from the paper [5].

According to the author's works cited in [5] internal correlation among all the geospheres is conditioned by means of water-and water-contenting mass fluxes, permanently formed at the inter-phase boundary between liquid core and lower mantle and penetrating through the whole open thermodynamic system the Earth-atmosphere-internal space (see Fig. 1).

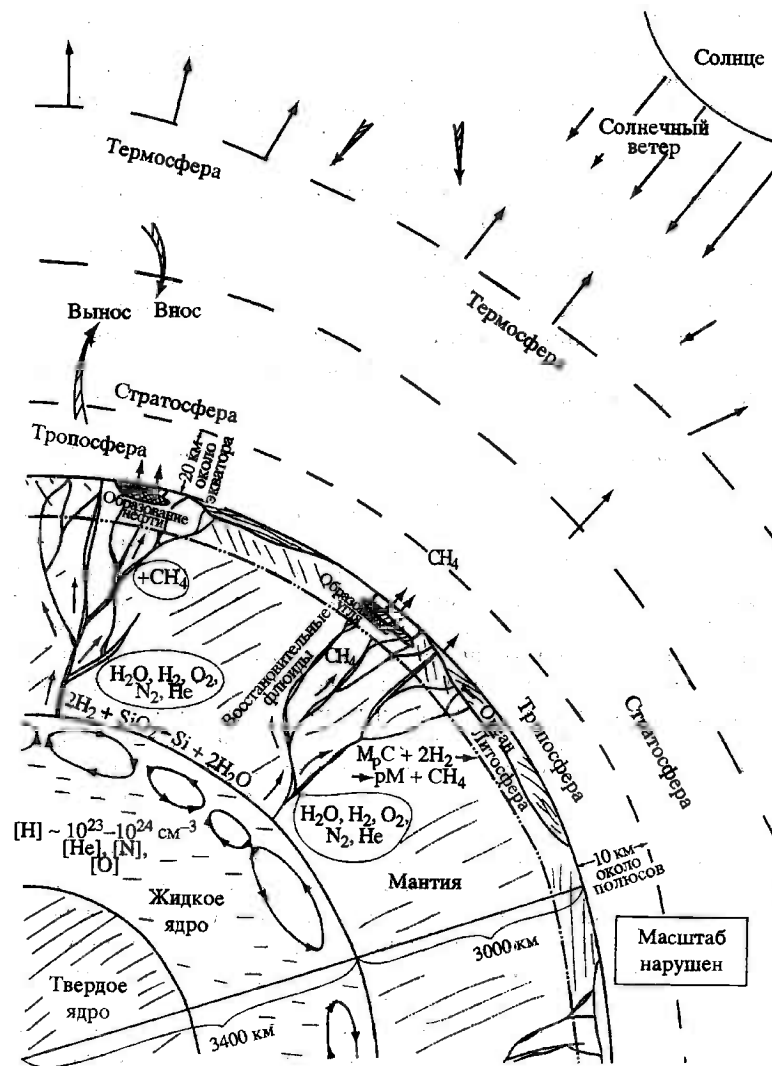
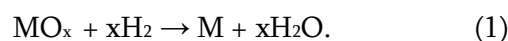


Fig.1. Mass fluxes in the geo-sphere's system [5].

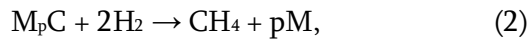
Initial state of the model – availability in Earth's liquid metal core solved hydrogen in high concentration of hydrogen penetrated into the Earth planetesimals as main component of the yang solar wind in the time of its forming 4.6 milliard years ago. It is suggested that the density of solved in liquid phase of the Earth core may arrive at  $0.1-1.0 \text{ g cm}^{-3}$  when mean density of liquid metallic core equals to  $\approx 10 \text{ g cm}^{-3}$ . Less quantity of He, N<sub>2</sub>, O<sub>2</sub>, ions of which were in the content of "young" Sun's solar wind, was dissolved in the liquid core (and in respective shares of fluids). On the basis of this hypothesis, the author discusses some following significant consequences; for example: (1) the chemical nature of the geomagnetism generation. Assumption about existence in liquid part of the Earth core of dissolved in it hydrogen opens possibility for generation of an etched magnetic field. At the boundary region of external melted metallic core of the Earth with the lower mantle the hydrogen being in atomic ionized state among catalytic active elements of Fe group and other heavy elements participates in endothermic chemical processes of restoration oxides MO<sub>x</sub> of the lower mantle (first of all, SiO<sub>2</sub>) with formation of water:



Forming products as well as leaking out from the core helium, carbon and other elements are taken aside along branchy system of hot plumes into adjacent to layers of lower mantle and lithosphere. At the same time, it is necessary to have in mind that the mantle is rebuilding heterogeneous dynamic system, layers of which are mixed each other (with character times of order tens and hundreds millions years) the convective flows catching on also the Earth crust, not only an oceanic but a continental one, too. This means that the system of hot plumes originating /proceeding from the boundary liquid core-lower mantle is rebuilding , replacing in the mantle system.

**2.2. Mixed inorganic and organic nature of carbon-contenting minerals** (see Fig.1) etc.

Contenting hydrogen and water restoring fluids, lead from interphasic boundary liquid core – lower mantle through (along) the hot plumes system, can interact with carbide of metals in lower and upper mantle forming methane:



**2.3. Fig. 1 is only qualitative picture of resulting fluxes of gases fluids** through the system of geospheres. By this scheme, the author wanted to emphasize that the Earth-atmosphere is open system and there are not irreversible circulations of water, carbohydrate, etc.). And under that decontamination of the Earth is persistently accomplished into the near space.

**III. It is considered the problem of influence of the spatial distribution of vegetation and soils on the prediction of cumulus convective rainfall.** In this review, the author uses published work to demonstrate the link between surface moisture and heat fluxes and cumulus rainfall. He, side by side other works, rather in detail, uses own works, especially extended account of in appendix, where the details of calculations are given in many short paragraphs. This heat energy can be derived from sensible heating at the Earth’s surface and from the release of heat as water vapor condenses or freezes. To develop into the cauliflower form of a thunderstorm cloud, the cloud air must be warmer than the surrounding air, such that the cloud air accelerates upward in a turbulent bubbly form [6].

**3.1. A surface energy and moisture budgets [6].**

The link between surface moisture and heat fluxes and cumulus convective rainfall: (a) the Earth’s surface role with respect to the surface energy and moisture budgets was examined; (b) changes in land-surface properties influence: (1) the heat and moisture fluxes within the planetary boundary layer; (2) convective available potential energy; (3) other measures of the deep cumulus cloud activity; (c) the influence of landscape patterning on the surface heating spatial structure – and producing focused regions for deep cumulonimbus convection; (d) development of obtained results from tropic to higher latitudes. While heat energy is the fuel for thunderstorms vegetation and soil govern the delivery of that energy and exert a strong influence on cumulus convective rainfall and thus on global weather and climate. The surface energy and moisture for bare budgets and vegetated soils during typical thunderstorm weather conditions (snow and ice are not considered in this discussion) are schematically illustrated apart from bare or vegetated soil, during thunderstorm weather conditions can be written as [6]

$$R_N = Q_G + H + L(E + T), \quad P = E + T + RO + I, \quad R_N = Q_S(1 - A) + Q_{LW\downarrow} - Q_{LW\uparrow}, \quad (4)-(5)-(6)$$

where  $R_N$  is the net radiation fluxes;  $Q_S$  is insolation;  $A$  is albedo;  $Q_{LW\downarrow}$  is downwelling longwave radiation;  $Q_{LW\uparrow} = (1 - \epsilon) Q_{LW\downarrow} + \epsilon\sigma T_s^4$  is upwelling long-wave radiation;  $\epsilon$  is the surface emissivity;  $T_s$  is the surface temperature;  $\sigma$  is the constant of Stefan-Boltzmann;  $Q_G$  is the soil heat flux;  $H$  is the turbulent sensible heat flux;  $L(E + T)$  is the turbulent latent heat flux;  $L$  is the latent heat of vaporization;  $E$  is evaporation (this term represents the conversion of liquid water into water vapour by the nonbiophysical processes, such as from the soil surface and from the surfaces of leaves and branches);  $P$  is the precipitation;  $T$  is transpiration (which represents the phase conversion to water vapour, by biological processes, through stoma on plants). Equations (4) and (5) are not independent of each other. A reduction in evaporation and transpiration in (5), for example, increases  $Q_G$  and/or  $H$  in (4) when  $R_N$  does not change. This reduction can occur, for example, if run off is increased (such as through clear cutting a forest). The precipitation rate, and type, also obviously influence how water is distributed between run off, infiltration, and the interception of water on plant surfaces. The relative amounts of turbulent sensible ( $H$ ) and latent heat fluxes ( $L(E + T)$ ) are used to define the quantity called the Bowen ratio ( $B$ ) and the evaporation fraction  $e_f$  are the relations (Seagal et al. (1988) [6]),

$$B = H/(L(E + T)), \quad e_f = L(E + T)/R_N; \quad H \approx (R_N - Q_G)/((1/B) + 1). \quad (7)-(8)$$

### 3.2. Consider schemes of the energy budget represented in Figs. 2a and 2b.

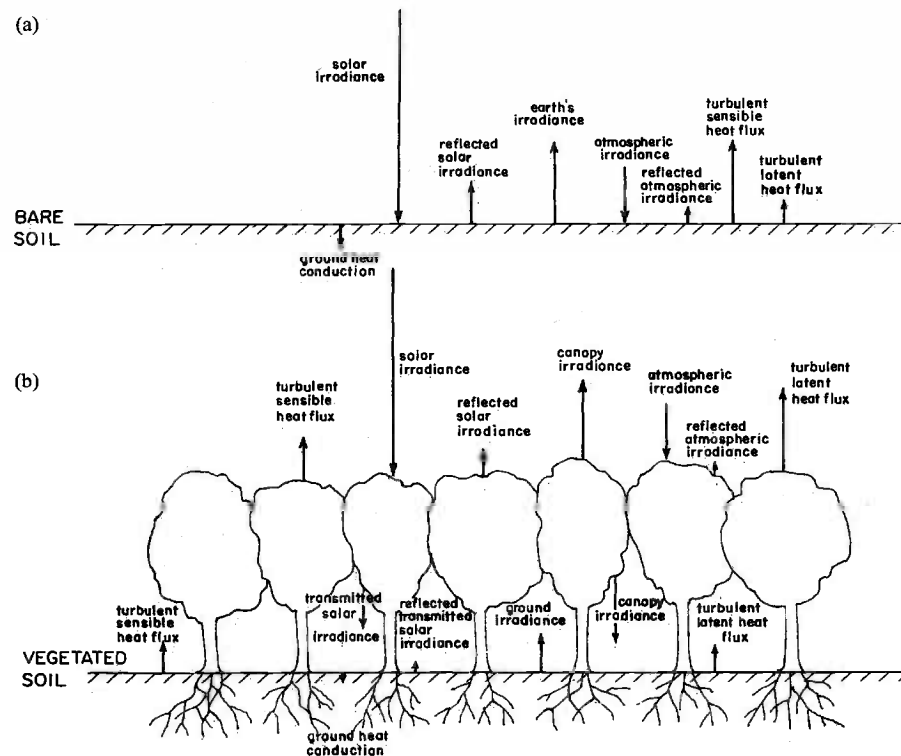


Fig. 2a. Schematic illustration of the surface heat budget over (a) bare soil and (b) vegetate land. The roughness of the surface (and for the vegetation, its displacement height) will influence the

magnitude of the heat flux. Dew and frost formation and removal will also influence the heat budget.

- (a) bare soil – solar irradiance↓, ground heat conduction↓, reflected solar irradiance↑, earth's irradiance↑, atmospheric irradiance↓, reflected atmospheric irradiance↑, turbulent sensible heat flux↑, turbulent latent heat flux↑;
- (b) vegetated soil – turbulent sensible heat flux↑, turbulent sensible heat flux↑, transmitted solar irradiance↓, solar irradiance↓, reflected transmitted solar irradiance↑, ground irradiance↑, reflected solar irradiance↑, canopy irradiance↑, canopy irradiance↓, atmospheric irradiance↓, reflected atmospheric irradiance↑, turbulent latent heat flux↑, turbulent latent heat flux↑.

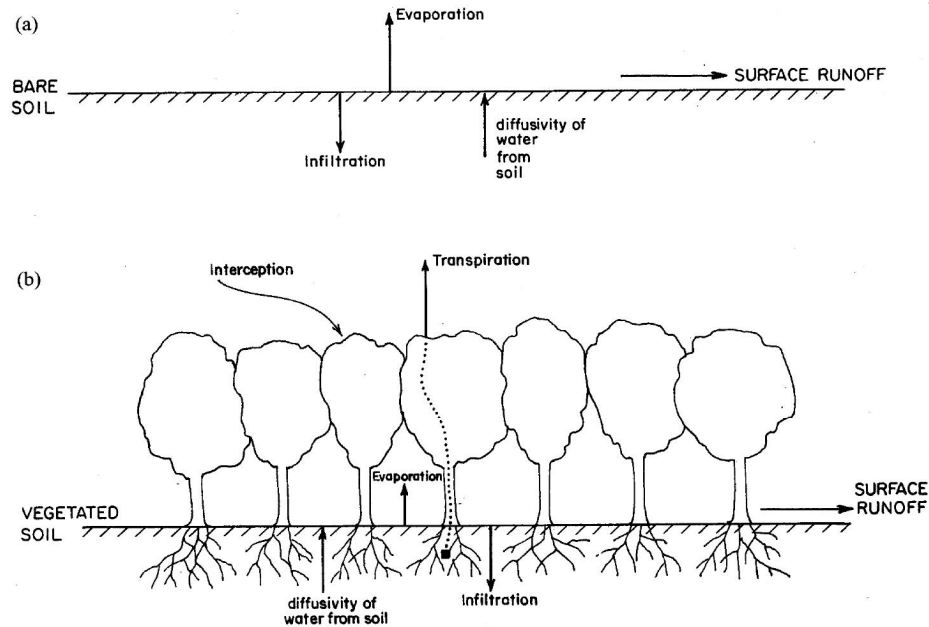


Fig. 2b. Schematic illustration of the surface moisture budget over (a) bare soil and (b) vegetate land. The roughness of the surface (and for the vegetation, its displacement height) will influence the magnitude of the heat flux. Dew and frost formation and removal will also influence the moisture budget.

- (a) bare soil – infiltration↓, evaporation↑, diffusivity of water from soil↑, surface runoff →;
- (b) vegetated soil – diffusivity of water from soil↑, interception↓, evaporation↑, transpiration↑, infiltration↓, surface runoff →.

Discussion of (7)-(8) by Segal et al. (1988, 1995) [6], when  $Q_G \ll H$  and  $E + T$ , show that  $H \approx [(1 + B)/B]^{-1} R_N$ , and thermodynamic **potential** for deep cumulus convection **increases**.

Therefore, any land use change that alters one or more of the variables in (4) and (5) will directly affect the potential for thunderstorm, and their resultant intensity, if they occur.

### 3.2. Boundary-layer effects [6].

**3.2.1.** Once **the surface energy budget** is altered, fluxes of heat, moisture, and momentum within the planetary boundary layer are directly affected. The author considers an idealized picture of the vertical structure of the convective boundary layer, where the surface heat flux  $H$ ,

depth of the layer  $Z_i$ , and the temperature stratification just above  $Z_i$ , determine the vertical profile of temperature and heat flux (Deardorff (1974)) and the entrainment of air from above  $Z_i$  to heights below  $Z_i$  are respectively given:

$$\partial Z_i / \partial t \sim H^{2/3} Z_i^{-4/3}, \quad H_{Z_i} = \alpha H, \quad (9)$$

where  $\alpha$  is the entrainment coefficient ( $\alpha \sim 0.2 \div 1.2$  (our suggestion)). The size of thermals generated from surface heating are a function of  $Z_i$ ,  $H$ , and height within the boundary layer. The rate of growth of the boundary layer during the day, and the ingestion of free atmospheric air into the boundary layer, are therefore both dependent on the surface heat flux  $H$ .

**3.2.2. A simplified form of the prognostic equation for  $\theta$**  can be used to illustrate how temperature change is related to the surface heat flux  $H_s$ ,

$$\frac{\partial \theta}{\partial t} = \frac{\partial}{\partial z} \left( \frac{H}{\rho C_p} \right), \quad (10)$$

where  $\rho$  is the air density,  $C_p$  – the specific heat at constant pressure. Integrating from the surface to  $Z_i$ , the depth of the boundary layer of  $H$ , using the mean value theorem of calculus yields [28]

$$\frac{\partial \bar{\theta}}{\partial t} = \frac{1}{\rho C_p Z_i} [H_s - H_{Z_i}] = \frac{1.2}{\rho C_p Z_i} H_s, \quad (11)$$

where  $H_{Z_i} = -\alpha H$ ,  $\alpha = 1.2$ . Using the equation a heating rate of a 1-km-deep boundary layer of  $2^\circ\text{C}$  over 6 hrs is produced by a surface heat flux of  $100 \text{ W m}^{-2} \approx 24 \text{ cal m}^{-2} = 2.4 \cdot 10^{-3} \text{ cal cm}^{-2}$ .

**3.2.3. Constructed on actual observations**,  $H$  (turbulent sensible heat flux) and other characteristics of the boundary layer, including  $Z_i$ , are altered as a result of different land-surface characteristics. Here they are:

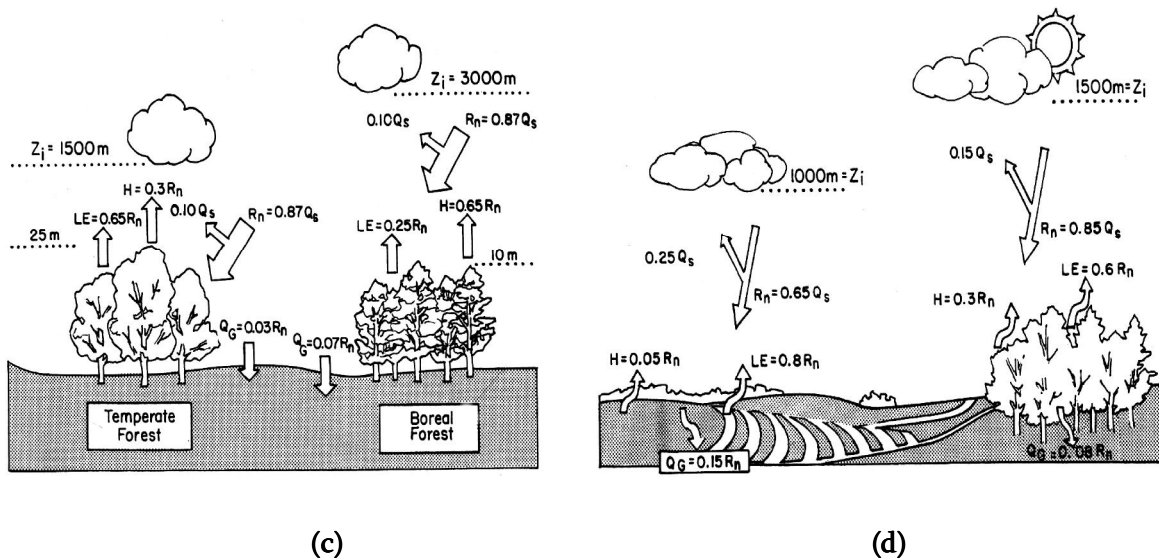


Fig. 2c. Schematic of the differences in surface heat energy budget and planetary boundary layer over a temperate forest and a boreal forest. The symbols used refer to eq. (4). Horizontal fluxes of heat and heat storage by vegetation are left out of the figure (P. Kabat (1999)) [6].

(a) temperate forest –  $Z_i = 1500$  m,  $\uparrow H = 0.3 R_N$ ,  $\uparrow LE = 0.65 R_N$ ,  $\downarrow R_N = 0.87 Q_S$ ,  $\uparrow R_N = 0.10 Q_S$ ,  $h_{\text{forest}} = 25$  m;  $\downarrow Q_G = 0.03 R_N$ ;

(b) boreal forest –  $Z_i = 3000$  m,  $\uparrow H = 0.65 R_N$ ,  $\uparrow LE = 0.25 R_N$ ,  $\downarrow R_N = 0.87 Q_S$ ,  $\uparrow R_N = 0.10 Q_S$ ,  $h_{\text{forest}} = 10$  m;  $\downarrow Q_G = 0.07 R_N$ ;

Fig. 2d. Same as Fig. 2c except between a forest and cropland (P. Kabat (1999))[6].

(c1)  $Z_i = 1000$  m,  $\uparrow H = 0.05 R_N$ ,  $\uparrow LE = 0.8 R_N$ ,  $\downarrow R_N = 0.65 Q_S$ ,  $\uparrow R_N = 0.25 Q_S$ ,  $h_{\text{forest}} = 0$  m;  $\downarrow Q_G = 0.15 R_N$ ;

(c2)  $Z_i = 1500$  m,  $\uparrow H = 0.3 R_N$ ,  $\uparrow LE = 0.6 R_N$ ,  $\downarrow R_N = 0.85 Q_S$ ,  $\uparrow R_N = 0.15 Q_S$ ,  $h_{\text{forest}} = 10$  m;  $\downarrow Q_G = 0.08 R_N$ .

Segal et al. (1989) discuss how wet soils and canopy temperatures affect the growth of the boundary layer. Amiro et al. (1999) measured elevations of surface radiometric temperatures by up to 6°C, which remained elevated even for 15 years, after forest fires in the Canadian boreal forest. The conclusion from the analyses in this section, and the associated references, is that the boundary layer structure, including its depth, are directly influenced by the surface heat and moisture fluxes.

3.2.4. Let us compare it with modelling one in our laboratory experiments. Value of heat flux equals to  $Q \approx 2 \text{ W cm}^{-2}$ , [1-4]; i.e. the modelling heat scale in our laboratory 80 time ( $\sim 100$ ) time more than in above considered nature case. Below, in last paragraph we return to this question once again. Since thunderstorms are an effective conduit for heat, moisture, and momentum to higher latitudes, landscape processes exert a major influence on global weather and climate. In the context of climate, soil and vegetation dynamics are as much a part of the climate system as are atmospheric variables. New observational platforms, such as the Tropical Rainfall Measuring Mission [Tao et al., 2001], offer opportunities to develop improvement understanding of the role of surface-atmosphere interactions on cumulus convective rainfall.

### 3.3. Global perspective.

The presence of the warm ocean surface conditions permits thunderstorms to occur there that would not happen with the average colder ocean surface. These thunderstorms export vast amounts of heat, moisture, and kinetic energy to the middle and higher latitudes, particularly in the winter hemisphere. This transfer alters the ridge and trough pattern, associated with the polar jet stream. This transfer of heat, moisture, and kinetic energy is referred to as “teleconnections”. Almost two thirds of the global precipitation occurs associated with mesoscale cumulonimbus and stratiform cloud systems located equatorward of 30°C. In addition, much of the worlds lightning occurs over tropical landmasses in the warm seasons, with maximums also over the midlatitude landmasses. These tropical regions are also undergoing rapid landscape

change. 1500-5000 thunderstorms (which are referred to as “hot towers”) are the conduit to transport this heat, moisture, and wind energy to higher latitudes. Thunderstorms occur only in a relatively small percentage of the area of the tropics, a change in their spatial patterns would be expected to have global consequences. On the rest of models see [6].

This paper demonstrates that vegetation and soil processes and change directly affect the surface energy and moisture fluxes into the atmosphere. This alteration in fluxes directly modifies the environment for thunderstorms. Since thunderstorms are in effective conduit for heat, moisture, and momentum to higher latitudes, landscape processes exert a major influence on global weather and climate. In the context of climate, soil and vegetation dynamics are as much a part of the climate system as are atmospheric variables. (About [6] important result the author of [7] notes that vegetation, owing to its ability to modify the surface energy balance, also affects convective activity and the development of the planetary boundary layer).

Then, in conclusion, the author **puts his hopes on new observational** platforms, such as the Tropical Rainfall Measuring Mission (TRMM) [8] offer opportunities to develop improved understanding of the role of surface-atmosphere interactions on cumulus convective rainfall. (!) Here **we make up our mind to** the model of this process by our **laboratory** bubble boiling method (LBBM) [1-3] (see below). There – rainfall TRMM-method, here – our bubble boiling original LBBM-method (see sect. 5.4).

### **3.4. Cumulus convection [7-9].**

The role of cumulus convection for hurricane circulation was examined in the review [7] with particular emphasis on mechanisms responsible for hurricane intensification. The potential for improved modeling of hurricanes and improved forecast of hurricane intensification is discussed. Above mentioned Smith’s review results [7] about hurricanes were considered by us in detail in paper [1], and Houze (2003), where he investigated the mesoscale convective systems, were used and critically analyzed by us in article [9], as stage works in natural convective studies.

## **IV. Vegetation as a dynamic component [7].**

4.1. Vegetation and climate are connected each other by modifying the energy, momentum, and hydrologic balance. Soil-vegetation-atmosphere transfer (SVAT) schemes explicitly consider the role of vegetation in affecting water and energy balance by taking into account its physiological properties, in particular, leaf area index (LAI) and stomatal conductance. These two physiological properties are also the basis of evapotranspiration parameterizations in physically based hydrological models. The paper’s aim: (1) to show the basic physical processes associated with the functioning of the terrestrial biosphere using simple nonbiogeochemical terminology, (2) to summarize used known parameterizations in models describing process-based vegetation and plant growth for including in SVAT schemes and hydrological models, and (3) to illustrate how these schemes and models would be accomplished (see Figs. 3a,b).

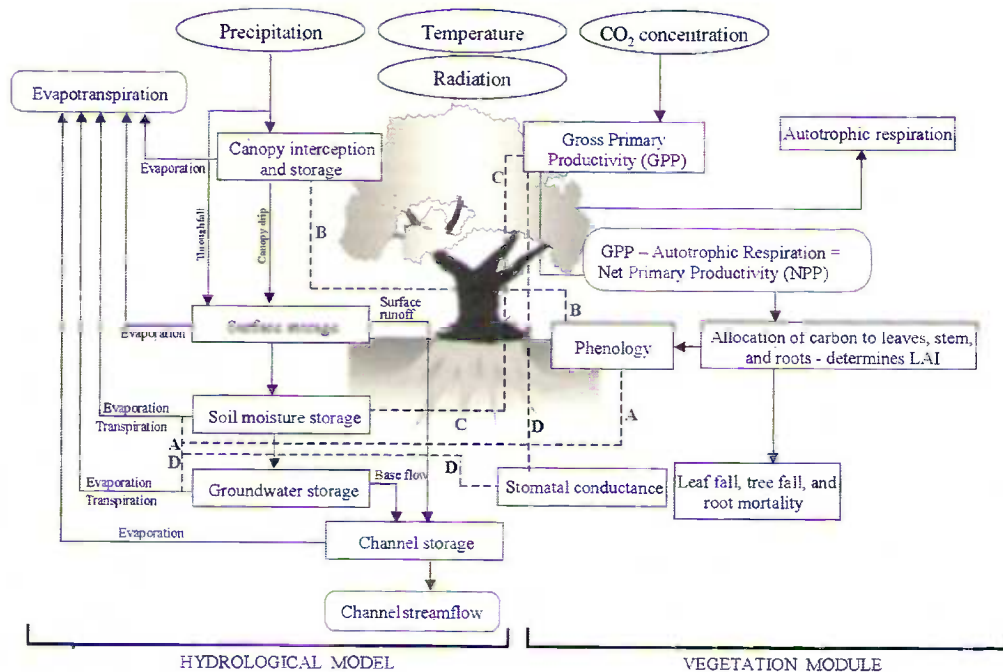


Fig. 3a. The manner in which the coupling between a dynamic vegetation module and a hydrologic model may be accomplished. The two primary variables exchanged between the two models are leaf area index and soil moisture. LAI (leaf area index) [7].

Dashed lines indicate linkages between the hydrological model and the vegetation module.

**A** – LAI affects transpiration from soil and groundwater stores.

**B** – LAI affects canopy interception, storage, and evaporation from canopy leaves.

**C** – soil moisture affects photosynthesis.

**D** – the coupling between photosynthesis and stomatal conductance is used to estimate transpiration.

---- indicates linkage between models.

**Hydrological model:** Precipitation↓, canopy interception and storage↓, canopy drip↓, throughfall↓, surface storage↓, surface runoff↓, soil moisture storage↓, groundwater storage↓, base flow↓, channel storage↓, channel streamflow. Canopy interception and storage (evaporation)↑, surface storage↑, soil moisture storage (evaporation, transpiration)↑, groundwater storage (evaporation, transpiration)↑, channel storage (evaporation)↑.

Precipitation, temperature, radiation CO<sub>2</sub> concentration – primary inputs.

Evapotranspiration, channel streamflow – primary outputs.

The others (in square brackets) – processes modeled.

**Vegetation module:** CO<sub>2</sub> concentration↓, gross primary productivity (GPP)↓, GPP – Autotrophic respiration = net primary productivity (NPP)↓, phenology, ←allocation of carbon to leaves, stem, and roots – determines LAI↓, → leaf fall, tree fall, and root mortality.

It is evident that represented schemes in Figures 1,2, and 3 of works [6, 7, 25] give us very interesting general and local picture about the role of thermodynamic processes in different geospheres. Even this brief review is enough for such conclusion. The primary vegetation

thermodynamic characteristics

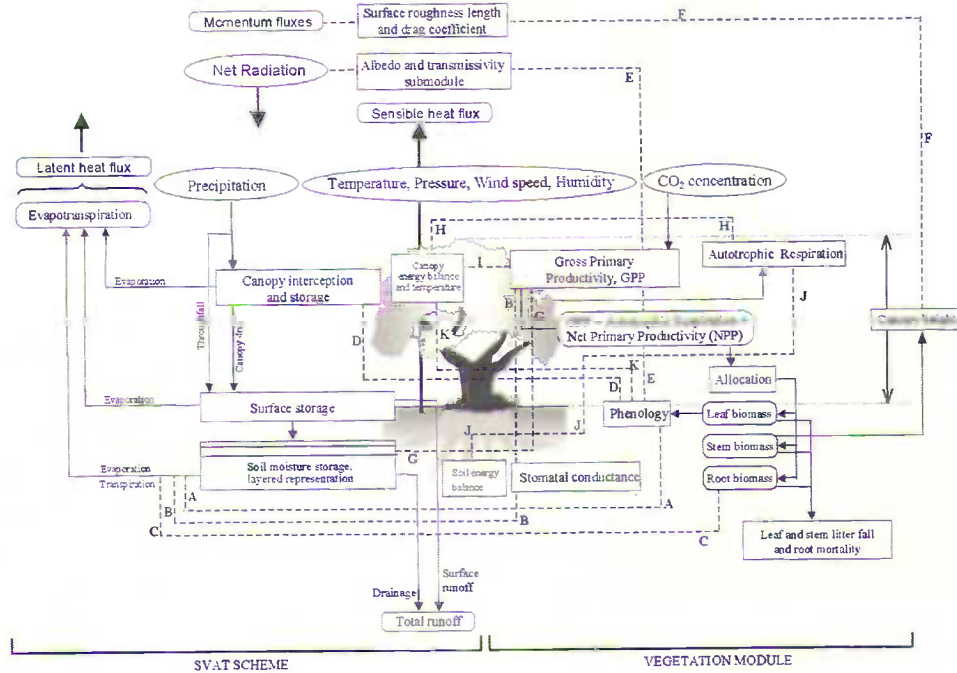


Fig. 3b. The manner in which the coupling between a dynamic vegetation module and a soil-vegetation-atmosphere transfer (SVAT) scheme may be accomplished. The primary variables exchanged between the two models include leaf area index, soil moisture, canopy temperature, roughness length, stomatal conductance, and root depth distribution [7].

Dashed lines indicate linkages between the hydrological model and the vegetation module.

A – LAI effects transpiration.

B – coupling between photosynthesis and stomatal conductance is used to estimate transpiration.

C – root biomass is used to estimate rooting depth and root distribution, and this affects transpiration.

D – LAI affects canopy interception, storage, and evaporation from canopy leaves.

E – LAI affects canopy albedo and transmittivity calculations.

F – canopy height affects surface roughness length, drag coefficient, and turbulent fluxes.

G – soil moisture affects photosynthesis.

H & I – canopy temperature affects leaf respiration and photosynthesis.

J – soil (energy balance and) temperature affects roots respiration.

K – LAI affects canopy energy balance and temperature.

**SVAT scheme:** net radiation↓, precipitation↓, throughfall↓, canopy interception and storage↓, canopy drip↓, surface storage↓, soil moisture storage, layered representation (drainage)→total runoff, surface storage (surface runoff)→total runoff. Temperature, pressure, wind speed, humidity → sensible heat flux, latent heat flux↑: canopy interception and storage (evaporation)↑, surface storage (evaporation)↑, soil moisture storage, layered representation (evaporation, transpiration)↑.

**Vegetation module:** CO<sub>2</sub> concentration → gross primary productivity, GPP; canopy energy balance and temperature → autotrophic respiration; GPP – Autotrophic respiration = Net primary productivity (NPP) → allocation (leaf biomass → phenology, stem biomass, root biomass) → leaf and stem litter fall and root mortality.

Thus, vegetation plays a significant role in influencing water and energy balance at the land surface via its effect on transpiration, interception, and the evaporation of precipitation from the canopy leaves. Vegetation, owing to its ability to modify the surface energy balance, also affects convective activity and the development of the planetary boundary layer [6]. The primary vegetation characteristics that affect water and energy balance are LAI, stomatal conductance, rooting depth, albedo, and surface roughness. The primary processes that need to be incorporated for modeling nitrogen dynamics include: (1) transfer of organic nitrogen from plant litter to the soil, (2) decomposition of organic nitrogen by microbes to yield mineral nitrogen, (3) uptake of mineral nitrogen by microbes and plants, and (4) leaching of mineral nitrogen by runoff. The physical processes of photosynthesis, respiration, allocation, and phenology, which are strongly dependent on environmental conditions, make vegetation a dynamic component. Incorporation of these processes in climate applications of SVAT schemes is necessary to model vegetation as an interactive component of the climate system, to understand the response of vegetation to changes in climate, and to assess the effect of changes in vegetation characteristics on the climate via the feedback processes.

## V. Comparison of different geophysical phenomena with each other. [14, 1-3]

5.1. Well-known in seismology universal scaling law describing the temporal decay of aftershock activity following an earthquake (modified Omori's law):

$$\frac{dN_{as}}{dt} = \frac{1}{t_0(1+t/t_1)^p}, \quad (11)$$

where  $N_{as}$  is the number aftershocks with magnitudes greater than a specified value,  $t$  is time measured forward from the occurrence of the main shock,  $t_0$  and  $t_1$  are constants, and the power  $p$  has a value near  $p \approx 1$ . When an earthquake occurs, there are regions where the stress is increased. This increase in stress is the fundamental cause of aftershocks. However, the systematic time delay before the occurrence of aftershocks requires an explanation: (a) stress corrosion- critical stress intensity; (b) subcritical crack growth; (c) empirically derived rate and state friction law; (d) the failure of composite and other engineering materials; (e) damage mechanics. Using (e) Main (2000), Shcherbakov and Turcotte (2003) have explained the power law decay of aftershocks. There appear to be fundamental similarities between aftershock delays and the nucleation of bubbles in a superheated liquid. These similarities led the authors (named in rf. [14]) to relate aftershock sequences to the power law scaling in the vicinity of a spinoidal line. This association is also supported by the relationship between the three-dimensional spatial distribution of aftershocks and the “backbone” of a three-dimensional percolation cluster given by Robertson et al. (1995)(see rf. [14]).

5.2. Van der Waals' diagram in seismology – Brittle fracture. [14].

We consider this question in the light of our laboratory bubble boiling method of modeling convective vertical two-phase motions in different above mentioned geophysical mediums.

Here it is considered the brittle failure of a solid phenomenon and association with statistical physics – the question which has received a great deal attention from engineers, geophysics, and physics [14]. For specialists in seismology the problem of earthquake scaling is the scaling of faults in the crust, more exactly statistical physics approach to understanding the multiscale dynamics of earthquake fault systems. They came to the conclusion that “these events can be regarded as a type of generalized phase transition, similar to the nucleation and critical phenomena that are observed in thermal and magnetic systems (Ma, 1976).”, – on the base of the Van der Waals-type equation of state.

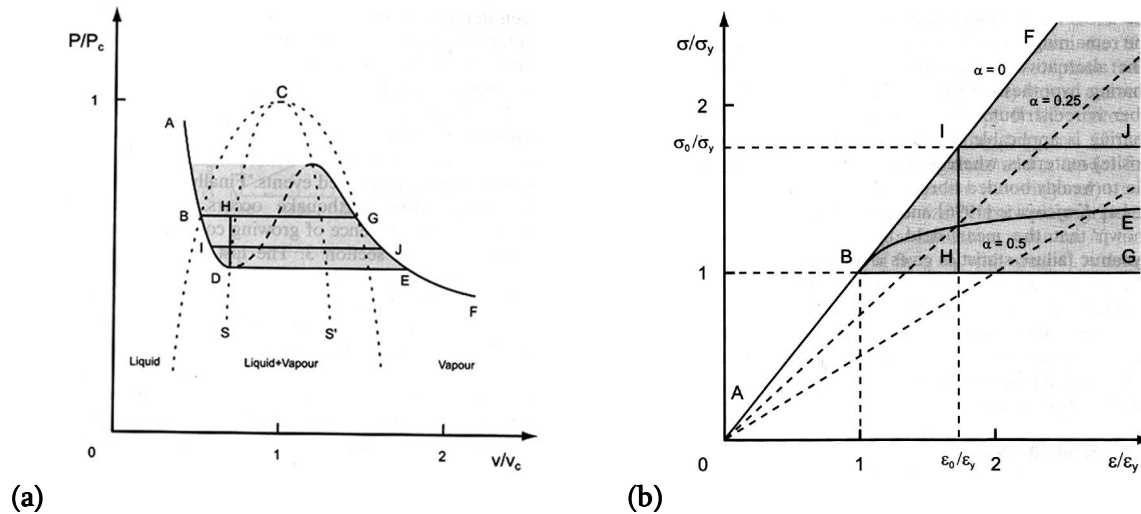


Fig. 4. **(a)** Schematic pressure-volume (P-V) projection of the phase diagram] of a pure substance (Debenedetti, 1996), The shaded region is metastable ; **(b)** Idealized stress-strain diagram for a brittle solid [14]. It is hypothesized that the solid behaves as a linear elastic material at stresses less than the yield stress  $\sigma_y$  and strains less than the yield strain  $\epsilon_y$  (path AB). Failure at an intermediate constant rate of stress increase takes place along path ABE. The dashed lines correspond to const values of the damage variable  $\alpha$ .

The equilibrium and non-equilibrium behaviors of the water-vapor mixture are discussed in the text [14]. According to our results the point B on the solid line ABE corresponds to our the second kind of discontinuity on above mentioned  $T(t)$ ,  $\Delta S(T)$  experimental curves (see [1-3]).

### 5.3. Brittle fracture [7].

The authors apply the concept of phase change to the brittle fracture of a solid. Let's a sample of area  $a$  is under compression by a force  $F$ . The state of the sample is specified by the stress  $\sigma = F/a$  and its strain  $\epsilon = (L_0 - L)/L_0$  is length and  $L_0$  is initial length. According to Hooke's law

$$\sigma = E_0 \epsilon , \quad (12)$$

where  $E_0 = \text{const}$  is Young's modulus.

Hypothesizing that a brittle solid will obey linear elasticity in the range  $0 \leq \sigma \leq \sigma_y$ , where  $\sigma_y$  is a yield stress, from (12) the corresponding yield strain is given by

$$\varepsilon_y = \sigma_y / E_0 . \quad (13)$$

If stress is applied infinitely slowly (to maintain athermodynamic equilibrium), one then hypothesize that the solid will fail at the yield stress  $\sigma_y$ . The failure path ABG in Fig. 4b corresponds to the equilibrium failure path ABG in Fig. 4a. This is equivalent to perfectly plastic behavior. The authors draw an analogy between the phase change behavior illustrated in Fig. 4a and the inelastic deformation of a solid illustrated in Fig. 4b. Pressure P is analogous to stress  $\sigma$ , and specific volume  $v$  is analogous to strain  $\varepsilon$ .

Pressure P is analogous to stress  $\sigma$ , and specific volume  $v$  is analogous to strain  $\varepsilon$ .

$$P \leftrightarrow \sigma, \quad v \leftrightarrow \varepsilon . \quad (14)$$

5.3.1. When the stress on a brittle solid is increased at a constant finite rate, linear elasticity (12) is applicable in the range  $0 \leq \sigma \leq \sigma_y$ . At stresses greater than the yield stress,  $\sigma > \sigma_y$ , damage occurs in the form of microcracks. This damage is accelerated strain and a deviation from linear elasticity. A typical failure path ABE is shown in Fig. 4b. In order to quantify the deviation from linear elasticity the damage variable  $\alpha$  is introduced in the stress-strain relation

$$\sigma = E_0(1 - \alpha) \varepsilon . \quad (15)$$

5.4. Comparison with magnetic systems [7].

5.4.1. Magnetization M plays a role similar to the density  $\rho$  in a liquid-gas system ( $M \leftrightarrow \rho$ ), and an applied external magnetic field h plays a role similar to the pressure P in liquid-gas systems ( $h \leftrightarrow P$ )

$$M \leftrightarrow \rho, \quad h \leftrightarrow P . \quad (16)$$

5.4.2. At the Curie point, large fluctuations in M are associated with the transition from ferromagnetism to paramagnetism and that these fluctuations are characterized by diverging length  $\xi$  and timescales  $\tau$ , respectively. Experiments indicate that  $\tau \propto \xi^z$ .

For diffusive systems  $z = 2$ , then

$$\tau \propto \xi^2 . \quad (17)$$

M and  $\rho$  are called the order parameters of the respective systems. These are the physical fields that respond to changes in the control parameters (T, h) or (T, P).

5.4.3. Away from the critical point (see ref. in [7]) phase transitions are first order and are associated with nucleation. In the water liquid-vapour system, nucleation is the process in which bubbles of water vapour form within liquid water prior to boiling. Changes in T and P can make a thermal system unstable to a change in  $\rho$ , leading to the appearance of a new phase. An example is the change of water from a liquid phase to a gas phase as T increased at constant P. In making the transition from the liquid to the gas phase, the mass of liquid water may progress from its stable equilibrium regime through a region of metastable liquid past the classical limit of

stability or spinoidal line. The existence of a spinoidal line is a consequence of the Van der Waals-type equation of state. It behaves like a line of critical points for the nucleating droplets of vapour. Near the spinoidal line, one observes divergent length scales  $\xi$  and time scales, as well as the appearance of large fluctuations in  $\rho$  and scaling as in the relationship  $\tau \propto \xi^z$ .

**VI. Laboratory experiments** of natural convective motions modeling by means of original bubble boiling method (LBBM) [1-3].

On the Fig. 5a graph  $T_{dc} = T_{kink} = 80^\circ\text{C}$ , and on Fig. 5b graph:  $T_{dc} = T_{kink} = 40^\circ\text{C}$ . In our experimental works [2, 3] at these (kink) temperatures, the experimental curves of entropy  $\Delta S(T)$  (see Fig. 6 in [2], and Figs. 1-6 in [3]) have more strong expressed character of dependence in range of temperature  $\Delta T_{kink} = 40^\circ \div 80^\circ\text{C}$ . These points of temperature (which represented in Fig. 6) show **change of the bubble boiling regimes in micro-scale size process (!)**.

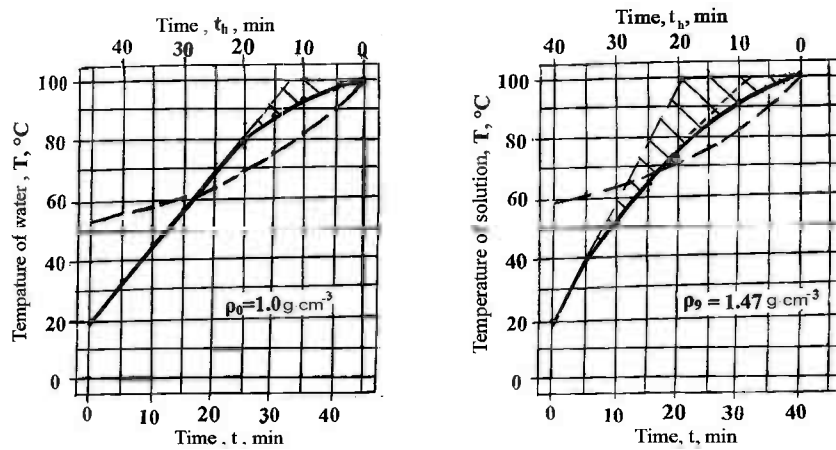


Fig. 5. The clear water (a) and sugar solution (b) bubble boiling (solid lines, time scale – below) and hysteresis (dashed lines, time scale – above) curves. Heat flux,  $Q(t) \approx 15 \text{ cal s}^{-1}$ . [3]

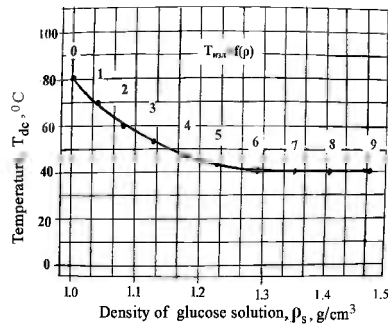


Fig. 6. Temperature of discontinuity,  $T_{dc}$ , dependence on the density of clear water ( $\rho_0 = 1.0 \text{ g/cm}^3$ ) and densities of the usual sugar solution ( $\rho_s, \text{ g/cm}^3, S = 1, 2, \dots, 9$ ) [2]

The authors of a paper [25] mentioned results of numerical experiments for **large-scale**, planetary size, global thermal convection rotating in atmosphere fluid system found a **kink** in the rate of entropy production **at a boundary between two different convection regimes**. (The sub-index

“kink” here is analogous of our sub-index “dc”, brief mark of term discontinuity of the second kind [1-3]). As we see, our laboratory bubble boiling method of modeling of a natural vertical convection [1-3] is in a good accordance with above mentioned global scale convection results [25] and also with ocean’s surface large scale turbulent mixed layer (see Appendix I [10], theory and Fig. I A). (Note, that more number of examples of vertical one-dimensional two-phase many-component motions of different geophysical fluids were considered in detail in [1]).

## VII. Analysis and discussion [1-3].

**7.1.** Having transfer to the question of heat capacity of fluid (at  $V = \text{const}$ ), it is necessary to note that theoretical task of calculation of heat capacity and its dependence from temperature, even for normal fluids, is unsolved, so far. A reason of that is in complexity of interaction among molecules with each other. As a rule, a heat capacity of the many-atomic liquids is increased with increase of temperature that perhaps is a reason of origin rotational motion and oscillations inside of the molecule itself. Inside of associated liquids part of heat of molecules is spent on their dissociation and as the number of complex molecules with increase of temperature is decreased so this part of heat capacity becomes smaller. Details are also given in our next article published in [3].

Named above decrease of heat capacity is added to its normal growth with increase of temperature – thus, the heat capacity of associated liquids passes over minimum (in case of clear water. As in case of gases, the heat capacity of liquids at constant pressure more than at constant volume, too. But equality  $C_p - C_v = R$  is not observed in case of liquids, because in time of their expansion the main role plays work against the forces of intermolecular interaction. In the case of ideal gas (for which this formula is obtained) that work equals to zero [16].

In our case a heat is added, which is spent on the bubble boiling process. That moment is seen in Fig. 5a,b on behavior of curves  $T(t)$  and  $\Delta S(T)$ , respectively, – the points of discontinuity of second kind on the boundary of change the bubble boiling regime from the smallest vapour bubbles to large ones. Here I must name the paper of Minobe et al. (2003) [20, 5] “which carried out numerical experiments of thermal convection in a rotating fluid system and found a kink in the rate of entropy production at a boundary between two different convection regimes. They suggested that the kink results from a preferred selection of a regime with a higher rate of entropy production. More direct evidence was recently obtained from numerical simulation of oceanic general circulation (Shimokawa and Ozawa, 2002). They found that irreversible changes always occur in the direction of the increase of entropy production. The numerical investigation is the subject of future studies, and the details will be reported on other occasions” [5].

**7.2.** We, independently, by means of laboratory experiments of modeling of natural convection, using chemical vessel where we boiled different water solutions. The solution was heated from below before intensive bubble boiling ( $T = 100^\circ\text{C}$ ). We obtain 1D, 2D, and 3D convections of bubble boiling – picture analogical the global picture published in directed papers. We suggested new method of modeling of natural process in laboratory conditions. Now I seek transferring coefficients for named above phenomena. In our case the change (transition) of regimes convection occur in interval ( $40^\circ\text{C} - 80^\circ\text{C}$ ) of temperature (slowing down) of entropy (fly up) to the maximal value of entropy-change-rate.

Numerical Method of Natural Convection [21, 5] → Bubble Boiling Convection Method [1-3] (NMNC)[20] → BBCM [1-3].

**7.3.** In global convection has been obtained very interesting result (Minobe et al., 2000), which is analogical to our experimental laboratory one. Numerical experiments [21] and laboratory

experiments [1-3] are opposed.

In our case [1-3], an added work (heat) is spent on the bubble boiling process – (fall of the rate of the temperature growth (at the temperature second kind discontinuity point,  $T_{\text{kink}}$ ) and rise of the rate of the entropy production growth with sensitive intensification of solution bubble boiling process (at the entropy second kind discontinuity point,  $\Delta S_{\text{kink}}$ ) – change of bubble boiling regimes from the smallest bubbles to the large ones.

**7.4.** [15] It is necessary to take into account two moments: a motion of molecules at heating and electrical interaction inside of molecules and among them. A liquid boils in the whole volume, and internal forces of ties are got over.

In our experiments, the bubble boiling of clear water,  $\text{H}_2\text{O}$ , begins intensively at  $80^\circ\text{C}$  (!). As is known from a theory of crystallography, amount of energy spent for heat of 1 gm of water equals to 1 cal, and to melt 1 g of ice at  $0^\circ\text{C}$  it is necessary 80 cal of heat, and for transformation of 1 g of water into vapour – 537 cal of latent heat at  $100^\circ\text{C}$ .

And vice versa, at the condensation of vapour of liquid large quantity of heat is released into an environment. If the water freezes, then were released such quantity of heat as during cooling of clear water from  $80^\circ\text{C}$  (the point of temperature and entropy the second kind of discontinuity of clear water [1-3]) to  $0^\circ\text{C}$ . Thus, the energy of molecular motion in crystal much less than in liquid phase. Would not this prove to be a key to the solution of the problem – why at low temperatures most of substances has right inner construction, i.e. crystal? From the other hand, the hysteresis point of view: what is occurred with molecules of cooling solutions? They will stop in most steady state positions with minimal free energy (because not the whole energy of molecules may attain in the process of the redistribution!). For the water served for a certain time as a solvent, in our experiments [1-3], it is necessary to take into account mainly electrical character of its molecules ( $\text{O}^-$ ,  $\text{H}^+$ ).

Most steady state will be distribution of hydrogen molecules in maximal nearness to the oxygen ones according to standard scheme leading to the origin of ice crystal. Electrical interactions forces, playing connective role in crystals, determine a type of their structure.

For example, one of the electrons from 11 electrons is the studied by us case of  $\text{NaCl}$ , having more simple structure than ice. An electron from 11 ones is easily come from  $\text{Na}$  atom, and atom of  $\text{Cl}$  takes for easily addition electron for formation full 18-electron shell instead of 17-electron one. Since 10 and 18 numbers of electrons form most stable configurations, the atom  $\text{Na}$  loses easily one electron, staying with 10, and atom  $\text{Cl}$  captures one electron for completion stable 18-electron configuration. As a result, positively charged atom  $\text{Na}^+$ , and negatively charged atom  $\text{Cl}^-$  form exceptionally (very) simple stable crystal structure which ones compare with 3D-chess-board [15].

## VIII. Conclusions

Thus, obtained experimental curves  $T(\rho)$ ,  $T(t)$  and  $\Delta S(T)$  (Figs. 1-6) (or the bubble boiling method) [3]: (1) – have universal character are independent on the substrate's nature and initial temperature of the researched solutions; (2) – allow one to establish the law of appearance of the points of the second kind discontinuities; (3) – give sufficiently full information about new results of provided experiments; (4) – may have independent and not only applied meaning; (5) – are significant from the point of view of opening perspectives of development and deepening of

suggested method; (6) –the method allows also to avoid superfluous technical efforts, quickly and without error, find main thermodynamic parameters of investigated solutions.

## APPENDIX I [10, 11]

### Surface mixed layer of a sea/ocean [10, 26, 1-4].

1. **Fig. IA** shows schematic picture of turbulent mixed layer of the surface of ocean caused by flux of thermals vertically directed because of Archimedes force. A useful law of vertical buoyancy transport was developed by the authors on the base of parcel theory [10].

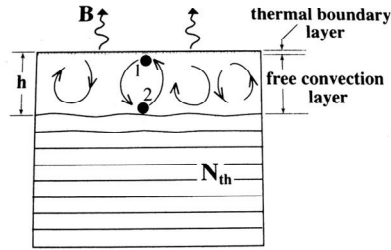


Fig. IA. A schematic diagram of a mixed layer [10].

(a) The thermal boundary layer may be thought of as being analogous conductive layer in laboratory convection between parallel plates, which communicates the boundary conditions from the plates to the interior of the fluid. The free convective layer, is given by well-known formula

$$\delta/h \approx 1/Pe^{1/2}, \quad (1A)$$

where Pe is a Peclet number,  $\delta$  is a depth of thermal boundary layer measuring the efficiency of buoyancy transfer on the plume. In the ocean  $Pe \sim 100$ ; that is, the plumes in the interior are much more efficient at transporting properties **vertically** than the turbulent elements that make up the thermal boundary layer near the surface is shallow  $\sim 100$ -200 m deep.

A useful “law” of vertical buoyancy transport can be developed using parcel theory as follows.

(b) Equations of thermal boundary layer in simplified standard form [11]. A heat flux density at the surface of the considered thermo-dynamical system

$$q_0 = \lambda \left. \frac{\partial \vartheta}{\partial y} \right|_0; \quad c_p \rho u \frac{\partial \vartheta}{\partial y}; \quad \lambda \frac{\partial^2 \vartheta}{\partial y^2}.$$

$$O(c_p \rho u \frac{\partial \vartheta}{\partial y}) = c_p \rho U_0 \frac{\theta}{L}, \quad O(\lambda \frac{\partial^2 \vartheta}{\partial y^2}) = \lambda \frac{\theta}{\delta_T^2}, \quad (2A)$$

$\theta$  – temperature on the external boundary of thermal layer. Into a boundary layer at the condition of equality both of heat fluxes  $q_0$  and convective intensity, we obtain following relations

$$c_p \rho U_0 \frac{\theta}{L} \approx \lambda \frac{\theta}{\delta_T^2}, \quad \frac{\delta_T^2}{L} \approx \frac{\lambda}{c_p \rho U_0}, \quad \left( \frac{\delta_T}{L} \right)^2 = \frac{a}{U_0 L}, \quad \frac{U_0 L}{a} = Pe, \\ \left( \frac{\delta_T}{L} \right)^2 \approx \frac{1}{Pe_0}, \quad \frac{\delta_T}{L} \approx \frac{1}{\sqrt{Pe_0}}. \quad (3A)$$

Now may compare (1A) and (3A) with each other.

1.1. We are also interested in results of experiments [26] connected with light solutions of NaCl , which has following kinetic parameters: temperature conductivity  $\xi_{\text{NaCl}} = 1.41 \cdot 10^{-3} \text{ cm}^2 \text{ s}^{-1}$ , diffusivity  $\delta_{\text{NaCl}} = 1.43 \cdot 10^{-5} \text{ cm}^2 \text{ s}^{-1}$ , kinematic viscosity  $\Upsilon_{\text{NaCl}} = 10^{-2} \text{ cm}^2 \text{ s}^{-1}$ . In particular, he studies many-component convection, and, by means of criterions of similarity, transfers them on the natural conditions [26].

1.2. In boiling water, fast moving vapour bubbles are supplied intensively from fixed points of sources, forming vertical oriented cylindrical form tubes (pillars) of merged vapour bubbles [1-4]. Such picture (Fig.14, [10]) was observed in our laboratory modeling experiments by bubble boiling method [1-4].

1.2. Fragments from [27].

Investigations of convective regime were begun after Benard's experiments in 1901. Theoretical investigation of this question was begun by Rayleigh, Lord (1916) who introduced an idea of critical number (Rayleigh's number) at which an instability is established in the thermodynamic system. Obtained above non-dimensional thickness of the boundary layer (3A) we may compare with Marshall's formula (1A). By means of the Rayleigh's number the wave length of convectively unstable mode is connected with the character depth of the liquid.

The Brown notes about necessity of the experimental (laboratory) modeling of natural convective flows[27]:

(1) Following investigation of convective regime, applicable to the geophysical phenomena, is hindered for lack of suitable experimental data (!); (2) Because the problem of convection is very far from a solution, one is obliged to have a subordinate character to the dynamical processes; (3) Necessary modification of existing theoretical models is rather simple but requires knowledge of number coefficients, which don't obtained very safely according to experimental data; (4) A great deal of external parameters and **shortage of experimental data** create main difficulties at analyzing of stratified boundary layer

**APPENDIX II.** Anti-similar figures: droplet-air bubble.

(a). Freely falling water/ice particle of precipitation in a cloud/atmosphere

$$\frac{4}{3} \pi r^3 \rho_{w,i} g = \frac{1}{2} C_D \rho_a v^2 S, \quad (6A)$$

(b). Air/vapour bubble motion in water.

$$\frac{4}{3} \pi r^3 \rho_{bb} g = \frac{1}{2} C_D \rho_w v^2 S, \quad S = 4\pi r^2. \quad (7A)$$

(c). Schematic calculation of an osmotic pressure [18].

$$PV = nRT, C = m/V\mu, P = CRT, P = \frac{C\mu RTn}{m}, P = \frac{1}{3} nm \overline{v^2} = nkT, \quad (8A)$$

$m$  is a mass of dissolved matter,  $n$  is a number of dissolved matter in  $1 \text{ cm}^3$  of the solution,  $k$  is the Boltzmann's constant.

(d). The temperature of intensive bubble boiling of solution of NaCl is higher than respective intensive bubble boiling of clear water  $\text{H}_2\text{O}$ . The Vant-Hoff's pressure, increase of the NaCl water solution the of intensive bubble boiling temperature are respectively following  $P_{\text{ocm}} = nkT$ ,  $\Delta t_{\text{NaCl}} \approx 8^\circ\text{C}$ ,  $P_{\text{ocm}} = n_{\text{NaCl}} k \Delta t$  [16]. In case of usual sugar,  $\text{C}_{12}\text{H}_{22}\text{O}_{11}$ ,  $\Delta t_{\text{sugar}} = 0$ .

**APPENDIX III.** Below represented variances of structures of NaCl crystal we chose to demonstrate an influence of the Earth gravitational field influence on the vertical orientation of its symmetry axe's (as in well-known case of the Archimedes force directed against the force of gravitation, too). For comparison of exceptional simple of NaCl molecule structure (1)-(2) with very complex one of the sugar (3), we represented these structure's symbols from [16].

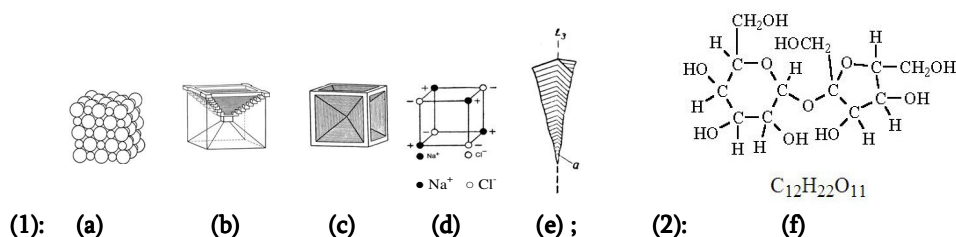


Fig. IIIA. (1) Usual salt crystallographic schemes [15, 16]; (2) – usual sugar chemical structure [INT-T].

(1)–NaCl crystal structures: (a)–(b)–(c)–(d)–(e); in (a) – small balls – ions  $\text{Na}^+$ , large balls – ions  $\text{Cl}^-$ ; in (d) – dark balls – ions  $\text{Na}^+$ , large balls – ions  $\text{Cl}^-$  [3], (2) (f)– $\text{C}_{12}\text{H}_{22}\text{O}_{11}$ .

Note on the form of NaCl crystal's (e)-case all, infinite order, symmetry axis of which directed vertically upwards in a gravity field (!) [16]. This, (e), and other vertex form crystals in light of the Curie's Vertex form will be at the centre of our attention. According to the memories of Maria Curie, P. Curie considered symmetry "as a state of space, characteristic for medium where this phenomenon is accomplished". For definition of this condition, pointed out P. Curie, it's necessary not only fully realize about state of it, but also about state both of motion and physical factors acting on it [29]. Untimely and dramatic disease in 1906 did not allow him to give developed wording of discovered by him universal principle of symmetry.

In connection of this, see the paper [Lemmleyn G. G. DAN SSSR, t. 33, № 6, 1941] about the form of a quartz and Grigoryev D. P. [Transect. of West All-Unoin mineralog. soc., part 76, iss. 1, 1947].

## References

- [1] Gvelesiani A. J. On the one-dimensional two-phase/many-component convective flows in different geophysical mediums: laboratory method of modeling of fluids bubble boiling. Georgian Geophys. Soc., 2013, v.16B, pp. 119-128.
- [2] Gvelesiani A., Chiabrishvili N. Laboratory modeling of thermals generation in geophysical environments by means of fluid bubble boiling method. J. Georgian Geophys. Soc., 2013, v.16B, pp. 129-137.
- [3] Gvelesiani A., Chiabrishvili N. Additional experiments about investigation of the peculiarities of the bubble boiling of clear water, H<sub>2</sub>O, and sugar, C<sub>12</sub>H<sub>22</sub>O<sub>11</sub>, and edible salt, NaCl, water solutions of different densities. J. Georgian Geophys. Soc., 2014, v.17A, pp.
- [4] Gvelesiani A., Chiabrishvili N. Definition of admixture mass content density of Tbilisi thermal waters by the new laboratory fluids bubble boiling method. J. Georgian Geophys. Soc., 2014, v. 17B, pp.
- [5] Timashev S. F. On the base principles of “New dialog with nature”. Problems of geophysics of the 21<sup>st</sup> century, I book, RAN OIFZ im. O.Yu.Shmidta. M.: Nauka, 2003, pp. 104-141.
- [6] Pielke R. A. Sr. Influence of the spatial distribution of vegetation and soils on the prediction of cumulus convective rainfall. Reviews of Geophysics, 39, 2 / May 2001, pp. 151-177.
- [7] Arora V. Modeling vegetation as a dynamic component in soil-vegetation-atmosphere transfer schemes and hydrological models. Reviews of Geophysics, 40, 2 / June 2002, pp. 1-26.
- [8] Smith R. K. The role of cumulus convection in hurricanes and its representation in hurricane models. Reviews of Geophysics, 38, 4 / November 2000, pp. 465-489.
- [9] Gvelesiani A. I. On the convective motions in different geophysical media. J. Georgian Geophys. Soc., 2012, v.15B, pp. 52-64.
- [10] Marshall J., Schott F. Open-ocean convection: observations, theory, and models. Reviews of Geophysics, 37, 1 / February 1999, pp. 1-64, 98RG02739
- [11] Gukhman A. A. Using of similarity method theory to the study of heat-mass processes exchange. M.: Vysshaya Shkola, 1967, 304 pp.
- [12] Roberts M. J., Jökulhlaups: A reassessment of floodwater flow through glaciers. Reviews of Geophysics, 2005, 43, RG1002/ 2005, pp. 1-21..
- [13] Jellinek A. M., Manga M. Links between long-lived hot spots, mantle plumes, D<sup>''</sup>, and plate tectonics. Reviews of Geophysics, 2004, v. 42, RG3002, pp. 1-35.
- [14] Rundle J. B. , Turcotte D. L., Shcherbakov R., Klein W., Summis Ch. Statistical physics approach to understanding the multiscale dynamics of earthquake fault system. Reviews of Geophysics, 2003, v. 41, N 4, RG4001, pp. 5.1-5.30.
- [15] Bunn Ch. Crystals: their role in nature and in science. 1964, Academic Press, New York and London. (1970, M.: Mir, pp. 312 (in Russian))
- [16] Shafranovsky I. I. Lectures on crystals-morphology. 1968, M.: Vysshaya Shkola, 174 pp.
- [17] Popov G. M. Shafranovsky I. I. Crystallography. M.: Vysshaya Shkola, 352 pp.
- [18] Pavlov V. I. Mechanics. Molecular physics. M.: GTTL, 1955, 356 pp.
- [19] Wallis G. B. One-dimensional two-phase flow. McGraw-Hill. Book Company. New York et al.(1972, M.: Mir, 440 pp.) (in Russian).
- [20] Advances in Heat Transfer. (Eds Irvine T. F., Jr, Hartnett J. P.), 1964, v. 1, Academic

- Press-New York-London (Problemy Teploobmena, 1967, M.: Atomizdat, 336 pp.) (in Russian).
- [21] Tao W.-K. J., S. Lang, W. S. Olson, R. Meneghini, S. Yang, J. Simpson, C. Kimmerow, E. Smith, and Halverson J. Retrieved vertical profiles of latent heat release using TRMM rainfall products. *J. Appl. Meteorol.*, 2001.
- [22] Minobe S., Y. Kanamoto, N. Okada, H. Ozawa, and M. Ikeda. Plume Structures in Deep Convection of Rotating Fluid. *Nature*, 2000, 19, pp. 395-396.
- [23] Schimokawa S., Ozawa H. On the thermodynamics of the oceanic general circulation: Irreversible transition to a state with higher rate of entropy production. *Q. J. R. Meteorol. Soc.*, 2002, 128, pp. 2115-2128.
- [24] Gvelesiani A. I. On the convective motions in different geophysical mediums. *J. Georgian Geophys. Soc.*, 2012, v.15B, pp. 52-64.
- [25] Ozawa H., Ohmura A., Lorenz R. D., Pujol T. The second law and the global climate system: a review of the maximum entropy production principle. *Reviews of Geophysics*, 41, 4 / December 2003, pp. 1-24.
- [26] Chashechkin Yu. D. Dissipative effects in hydrodynamics of non-homogeneous geosphere. *Problems of geophysics of the 21<sup>st</sup> century, First book. RAN OIFZ im. O. Yu. Shmidta. M.: Nauka, 2003, pp. 66-103.*
- [27] Brown R. A. Analytical methods in planetary boundary-layer modeling. Adam Hilger, London, 1972 (Russian ed., Leningrad: Gidrometeoizdat, 1978, 150 pp.)
- [28] Smokowski E. W. Calculus with analytic geometry. Prindle, Weber & Schmidt, Boston, Massachusetts. Second edition, 1979, 1085 pp.
- [29] Curie M. Pier Curie. *Nauchn. khim.-tekhn. Izd., Leningrad, 1924.*

(Received in final form 30 August 2014)

## **Ria Termodinamikuri geofizikuri sistemebi: konveqcia da mismagvari procesebis modelireba siTxis buStovani duRilis meTodiT**

anzor gvelesiani

rezieme

svadasxva geofizikur areSi gagrZelebulia konveqciuri moZraobebis ganxilva [1-3] SemoTavazebuli buStovani duRilis meTodiT maTi modelirebis TvalsazrisiT. buStisebri duRilis meTodi misaRebia: (a) globaluri planetaruli masStabis cirkulaciis [5]; (b) okeaneSi zedapiruli Serevis fenis [10]; (g) analogiisa qanebSi mikrobzarebis gaCenis Semdgom msxvrevs da buStebis Canasaxebis Semdeg siTxis duRilis Soris [14]; (d) yinulovani CrdiloeTis Termaluri wylebis (geizerebis) [12]; (e) dedamiwis magmis da sxv. [22, 23] eqsperimentuli kvlevis Sedegebis energetikuli analizi da meTodis dazusteba mosalodnelia uaxloes SromebSi.

# **Открытые термодинамические системы: моделирование конвекции и подобных явлений единым методом пузырькового кипения жидкости**

Анзор Гвелесиани

Резюме

Продолжено рассмотрение конвективных движений в различных геофизических средах с точки зрения их моделирования методом пузырькового кипения, предложенным в [1-3]. Метод пузырькового кипения жидкости с целью моделирования вертикальной одномерной, и трёхмерной конвекции в лабораторных условиях оказывается приемлемым при рассмотрении: (а) глобальной, планетарного масштаба, циркуляции [5]; (б) поверхностного слоя смешения океана [10]; (в) аналогии между микротрещинами, ведущими к разрушению горных пород, и пузырьковым ядрообразованием, ведущим к кипению [14]; (г) особенностей термальных вод в ледниковых северных районах [12]; (д) магмы Земли и др. [5, 22, 23]. Энергетический анализ и уточнение деталей метода предполагаются в ближайших работах.